Studying the performance of various polymeric ultrafiltration membranes in dye removal

Mohammed M. Hassan[a], Zaidun N. Abudi[a], Mustafa H. Al-Furaiji[b],*

[a]*Environmental Engineering Department, College of Engineering, Mustansiriyah University, Iraq, Tel.: 009647712232069;*
email: eng.mmh1987@gmail.com (M.M. Hassan), Tel.: 009647826127800; email: zaidun.naji77@uomustansiriyah.edu.iq (Z.N. Abudi)
[b]*Environment and Water Directorate, Ministry of Science and Technology, Baghdad, Iraq, Tel.: 009647736792156;*
emails: alfuraiji79@gmail.com (M.H. Al-Furaiji)

ABSTRACT

In this study, flat-sheet membranes were fabricated by phase inversion method, using four types of polymers (i.e., polysulfone (PSU), polyethersulfone, polyvinylidene fluoride, and polyacrylonitrile (PAN)) with different concentrations (13, 15, and 17 wt.%) in dimethylformamide solvent for the ultrafiltration application in dye removal. The characteristics of membranes were investigated using Fourier-transform infrared spectroscopy, atomic force microscopy, scanning electron microscopy, dye removal, water permeation flux, and porosity. Two different dyes (i.e., Malachite green and Congo red) were studied at a concentration of 100 ppm. The results showed that membranes with a concentration of 17% had the best performance in the water flux rate and dye rejection. Significantly, the PSU 17% membrane is the optimal membrane where the permeate rate is in the range of 8.06 L/m^2·h at 2 bar and 52.97 L/m^2·h at 7 bar for the Malachite green dye and 10.96 L/m^2·h at 2 bar, and 58.96 L/m^2·h at 7 bar for Congo red dye. The effect of the polymer concentration on the membrane properties was investigated extensively. The dye rejection for the PSU 17% membrane was recorded at 98.04% and 93.02% for Malachite green dye, and 99.42% and 98.59% for Congo red dye were pressures at 2 and 7 bar, respectively. The outcomes of this paper can help in choosing the best polymer and conditions to remove dyes from wastewater.

Keywords: Polysulfone; Polyethersulfone; Polyacrylonitrile; Polyvinylidene fluoride; Ultrafiltration membrane; Dye rejection; Phase inversion

1. Introduction

Dyes are used to color products in various industries, including textiles, leather, cosmetics, paper, printing, plastic, medicines, and food [1]. Removing dyes using cutting-edge, very effective methods is essential because this effluent frequently contaminates water and is quite harmful [2]. Established treatment methods are currently used to remove dyes from industrial wastewater, such as adsorption [3], chemical oxidation [4], coagulation/flocculation [5], ozonation [6], biological treatment [7], electrocoagulation [8], advanced oxidation process [9], and photocatalytic degradation [10]. This latter technique is frequently employed to address synthetic chemical dyes, such as Crystal violet dye [10]. In order to treat dyes in an aqueous solution, Chham et al. [11] used a natural adsorbent based on Moroccan bituminous shale in an adsorption method (case of methylene blue). The electrocoagulation technique has been proven to be an effective and affordable approach for treating wastewater from the textile industry, according to Daij et al. [8]. However, it has been demonstrated to be insufficient because these dyes' chemical architectures prevent biodegradation [12]. Membrane separation technology is one of the most promising techniques

---

* Corresponding author.

for wastewater treatment and high-quality water production [13]. This significance of membrane application lies in several benefits, such as high efficiency, minimal impact on the environment, lack of chemical use, and simplicity of handling [14]. This technology has various applications in the pharmaceutical industries [15], the agro-food industries [16], water treatment [17], and industrial effluents, the chemical, electronic and nuclear industries, desalination [18], gas separation [19], medicine [20], as well as seawater desalination [21]. Some of these membrane processing techniques include reverse osmosis (RO), nanofiltration (NF), microfiltration (MF), and ultrafiltration (UF). The past few decades have seen an increase in interest in ultrafiltration technology because of its many advantages, such as its lack of phase shifts, low operating pressures, and ambient or extremely low operation temperatures [22].

Numerous membrane materials, particularly polymers, have been employed to create UF membranes, including polyvinylidene fluoride (PVDF) [23], polysulfone (PSU) [24], polyacrylonitrile (PAN) [25], and polyethersulfone (PES) [26]. Polymer materials are the most essential and cost-effective materials utilized on a large scale to create membranes, and its properties may be easily adjusted to meet specific needs. Polymers offer numerous alternatives for membrane formation [27]. Despite being readily available commercially, these polymer materials' limited industrial application is due to their poor permeation flux and fouling problems. Researchers have developed numerous strategies, such as the utilization of polymer blends, to enhance the functionality of polymeric membranes [28], incorporating nanoparticles [29,30], and graft copolymerization with free radicals (chemical modification) [31]. Al-Ani et al. [28] suggested a new strategy to improve membrane performance by blending polyethersulfone (PES) with polyphenylsulfone (PPSU). Remove Acid black 210 dye from simulated effluent from the leather tanning industry at concentrations of 35, 45, and 65 ppm. PPSU-PES ultrafiltration membranes were created using the traditional phase inversion approach. PES concentrations of 0, 4, 5, and 6 wt.% were examined, while the concentration of PPSU remained constant at 20%. It was discovered that the membrane's structural shape changed depending on the PES concentration, and it was found that the permeation flux did not change with pH. Additionally, it was shown that the performance of membranes increased over those made from the plain PPSU membrane from 5.77 to 27.7 L/m²·h and 3.46 to 19.62 L/m²·h for distilled water and feed solution of 35 ppm, respectively. At the same time, the dye removal was higher than 99.65% for all of the membranes investigated [28].

Another study by Zinadini et al. [32] looked into the effects of combining a graphene oxide (GO) nanoplate with PES/polyvinylpyrrolidone (PVP) nanofiltration membranes in order to remove Direct Red 16 and filter powder milk. The PES treated with GO had the best dye removal performance. Additionally, Abedi et al. found that chemical surface modification considerably increased the fouling resistance of polyacrylonitrile (PAN) membranes [33,34].

This study aimed to fabricate membranes from various types of polymers (PSU, PES, PAN, and PVDF) with various concentrations (13, 15, and 17 wt.%) by the phase inversion method. Membranes were evaluated by structural morphology, permeability rate, and removal ratio. The results of this study can be valuable in obtaining a membrane used in ultrafiltration membrane applications and thus removing dyes from wastewater. Also, this paper can help in choosing the best polymer and concentration to prepare the best membrane for dyes removal application.

2. Materials and methods

2.1. Materials

Different membrane materials were used in this work such as polysulfone (PSU, MW = 35,000 g/mol), polyethersulfone (PES, MW = 58,000 g/mol), polyacrylonitrile (PAN, MW = 150,000 g/mol), and polyvinylidene fluoride (PVDF, Mw = 534,000 g/mol). All polymers were from Xian Lyphar Biotech, China. N,N-Dimethylformamide (DMF, $HCON(CH_3)_2$, MW = 73.10 g/mol) from Ambernath, India, was used as the polymer solvent. Malachite green dye [chemical formula = $C_{52}H_{54}N_4O_{12}$, MW = 927.02 g/mol] was obtained from Alpha Chemika, India, and Congo red dye [chemical formula = $C_{32}H_{22}N_6Na_2O_6S_2$, MW = 696.7 g/mol] was ordered from BDH Chemicals Ltd Poole England, UK.

2.2. Membrane fabrication

Twelve polymer membranes were fabricated via the phase inversion method. The dried PES, PSU, PAN, and PVDF polymers at different concentrations (i.e., 13, 15, and 17 wt.%) were dissolved in N,N-Dimethylformamide (DMF) solvent. The magnetic stirrer used for the mixture was heated for 60°C and agitated for 6 h until a clear solution was obtained. The polymeric solution was left overnight to degassing. Then, an appropriate amount of the polymeric solution was poured on a clean glass plate which was then cast with a thickness of 180 μm using a casting knife. The phase inversion procedure was then completed by placing the constructed membrane into a deionized water bath at room temperature. Deionized water was used to repeatedly rinse the manufactured membranes, which were then kept in the water for at least 24 h before being used. The composition of the casting solutions for each membrane is listed in Table 1.

2.3. Membrane characterization

The membrane's chemical composition was investigated using a Fourier-transform infrared spectroscopy-attenuated total reflection (FTIR-ATR) spectrometer (PerkinElmer, Australia). FTIR with a resolution of cm⁻¹ in the range of 450–4,000 cm⁻¹ was used to describe it, and the median value was calculated using 50 scans. The prepared membranes' top membrane surface and cross-sectional morphology were examined using a scanning electron microscope (TESCAN VEGA3 SB instrument, EO Elektronen-Optik-Service GmbH, Germany) operating at a 5.00 kV accelerating voltage. Membrane samples were produced by sputtering the coating with a 0.5 nm film of Pd metal and drying the membrane at ambient temperature. In order

Table 1
Casting solution composition of the prepared membranes

	Casting solution (wt.%)	
Type of membranes	Polymer (wt.%)	DMF (wt.%)
PSU 13%	13	87
PSU 15%	15	85
PSU 17%	17	83
PES 13%	13	87
PES 15%	15	85
PES 17%	17	83
PAN 13%	13	87
PAN 15%	15	85
PAN 17%	17	83
PVDF 13%	13	87
PVDF 15%	15	85
PVDF 17%	17	83

to maintain the membrane structure, the membranes were broken into pieces and examined utilizing scanning electron microscopy (SEM) technology for cross-sectional imaging. At various magnifications, the membrane's cross-section and outside surface were scanned.

The surface morphology and roughness of the generated membrane were examined using an atomic force microscope (SPM AA300 Angstrom Advanced Inc., USA). A 1 cm² × 1 cm² membrane sample was sliced and mounted on the holder, where a 1 μm × 1 μm² area was scanned. The average roughness R_a and the root mean square height R_q were used to represent the surface roughness parameter.

The gravimetric technique was used to estimate the membranes' porosity, as indicated by Eq. (1) [35]:

$$\varepsilon = \frac{(W1 - W2)}{A \times T \times \rho} \times 100 \tag{1}$$

where ε is the porosity (%), W_1 is the wet membrane's weight (mg), W_2 is the dry membrane's weight sample (mg), A is the effective area of membrane (cm²), T is the thickness of the membrane (μm), and ρ is the water density (0.998 g/cm³ at 25°C). The membrane samples were left in distilled water at room temperature for 24 h. After wiping away any remaining water, each membrane was weighed. To estimate the average porosity of membranes, triplicates of each sample were tested.

The concentration of dyes in water was calculated using a UV-vis spectrophotometer (Pharo 300, Merck, Darmstadt, Germany)

2.4. Performance test

The permeation of the UF membranes in this study was evaluated under cross-flow filtration conditions. The apparatus setup was equipped with a membrane cell having an effective membrane area of 24 cm² (Fig. 1) to measure the water flux and dye rejection. Each membrane sample was pressurized under various cross-membrane pressures

(i.e., 2, 2.5, 3, 3.5, 4, 4.5, 5, 5.5, 6, 6.5 and 7 bar) at room temperature (25°C).

Malachite green and Congo red dyes separation tests were assessed at concentrations of 100 ppm in aqueous solutions to determine the membranes' removal efficiency. The water flux and dye rejection were calculated by Eqs. (2) [36] and (3) [37], respectively.

$$J = \frac{V}{A.t} \tag{2}$$

where J is the water flux of the membrane (L/m²·h), V is the produced volume (L), A is the surface area of the membrane (m²), and t is the time the permeate was collected (h).

$$R = \left(1 - \frac{C_p}{C_f}\right) \times 100 \tag{3}$$

where R is the dye rejection ratio, where C_f and C_p: are the concentrations of the dye in the feed solution and the permeate (mg/L), respectively.

3. Results and discussion

3.1. Membrane characterization

3.1.1. FTIR results

Fig. 2 shows the FTIR-ATR analysis that was conducted to compare the chemical compositions of the PSU 17% membranes before and after exposure to two different types of dye solutions and to assess the functional groups of the PSU 17% membrane.

The FTIR analysis was presented to determine the chemical compositions of the prepared membrane after the ultrafiltration application was performed using an aqueous solution containing 100 ppm of dye. Fig. 2A represents the pristine PSU 17% membrane, and Fig. 2B and C represent the PSU 17% membrane after permeation operation using Malachite green dye and Congo red dye, respectively. Each additionally contains the PSU support layer's spectrum. According to the literature, around 950 cm⁻¹ is the Si–OH stretching vibration [38], and the Si–O–Si peak measures about 1,050 cm⁻¹ [39]. The strong peaks at 3,898.23 for the pristine PSU 17% membrane, while 3,895.92 and 3,639.79 cm⁻¹ for PSU 17% membranes under testing using Malachite green dye and Congo red dye, respectively. It can be seen that there is a significant change in the FTIR analysis in Fig. 2B and C compared to Fig. 2A, which indicates the influence of the chemical composition of the membrane under operating conditions such as dye concentration and operating pressures in ranges 2 and 7 bar. And therefore increasing the number of spectral peaks due to the variable thickness of the dyeing layer on the surface of membranes.

3.1.2. SEM images

Membrane morphology is essential in studying the separation mechanisms, and it is affected by membrane casting solution viscosity, solvent-polymer interaction, solvent–non-solvent interdiffusion rate, and time and coagulation

temperature [40–43]. The morphologies of the membranes generated with various concentrations are depicted in Figs. 3 and 4. Diffusion allows the casting solution to undergo a phase transition, which is how the membrane is created. This phase transition is caused by the exchange of the solvent (DMF) and non-solvent (water) [22]. When the diffusion rate between the solvent and the non-solvent is low, a sponge-like structure occurs; however, the membrane only develops a finger-like shape at high diffusion rates [44,45].

Consequently, these changes are most likely due to the shift in the diffusion rate of the solvent and non-solvent as a result of the polymers' concentration changing. Another noteworthy point was that the polymer membranes with a concentration of 17% had a better pore structure than membranes at 15% and 13%. It is noted that the PSU 13% membrane has a more porous and spongy structure compared with the PSU 15% membrane, which has a denser, smaller pore size, and spongious phase. Increasing the concentration of PSU to 17% did change the general structure of the membranes and created a more stable structure of a leaf-like morphology. The SEM images of the membrane produced from PES 13% and PES 15% featured huge structural layers resembling fingers and sponges, with massive voids near the top surface. A thin finger-void layer resulted from increasing the PES concentration in the polymer solution up to 17%, where the shape of a sponge was more substantial along the uppermost layer of the surface. The microvoids in the dope solution enlarge at low polymer concentrations and are restrained at higher polymer concentrations [46]. When the higher compatibility between the solvent and non-solvent, phase inversion occurs as soon as the coagulation bath receives the solution film [47]. As a result, a porous structure with large cavities emerges.

If the non-solvent is incompatible with the solvent, the phase separation process is slower, and the structure of the membrane resembles a sponge [47]. Bigger cavities cause flux enhancement in the membrane [48].

As shown in Fig. 3, numerous dark spots in SEM images of the surface structure of PVDF membranes may make the top surface porous and not truly skin-like. Some valleys are only a few tens of nanometers wide, and some are submicrometer in size [49]. The number of highness and lowness on the membrane surface rises as the solution concentration increases, while their depth decreases [50,51]. For the casting solutions' 17% and 15% concentrations, circular pores were noticed in the discerning layer in the cross-section images. Several tiny pores could be seen, some of which may connect to the skin's deep microvoids. For PVDF 13%, the top surface comprises nanoscale granular objects whose dendritic structures can be seen. All PVDF membranes are characterized by nodules that vary in size and compactness. Because of the selective layer's increased concentration, the membrane's outer layer becomes thicker, substantially impacting the inner membrane structure.

The morphology of PAN membranes was compared, and SEM was used to observe the membrane's structural changes, as seen in Fig. 3. These membranes prepared by different concentrations (13, 15, and 17 wt.%) exhibited a typical asymmetric structure composed of separating skin layers and solid porous matrixes. When it comes to the penetration or retention of solutes, the skin layer is in charge, while the porous bulk serves as mechanical support. The PAN membrane in the concentration of 17% demonstrated a comparable impact on the membrane structures, composed of a thin layer of skin and a porous mass with independent dense tree roots-like. When the content
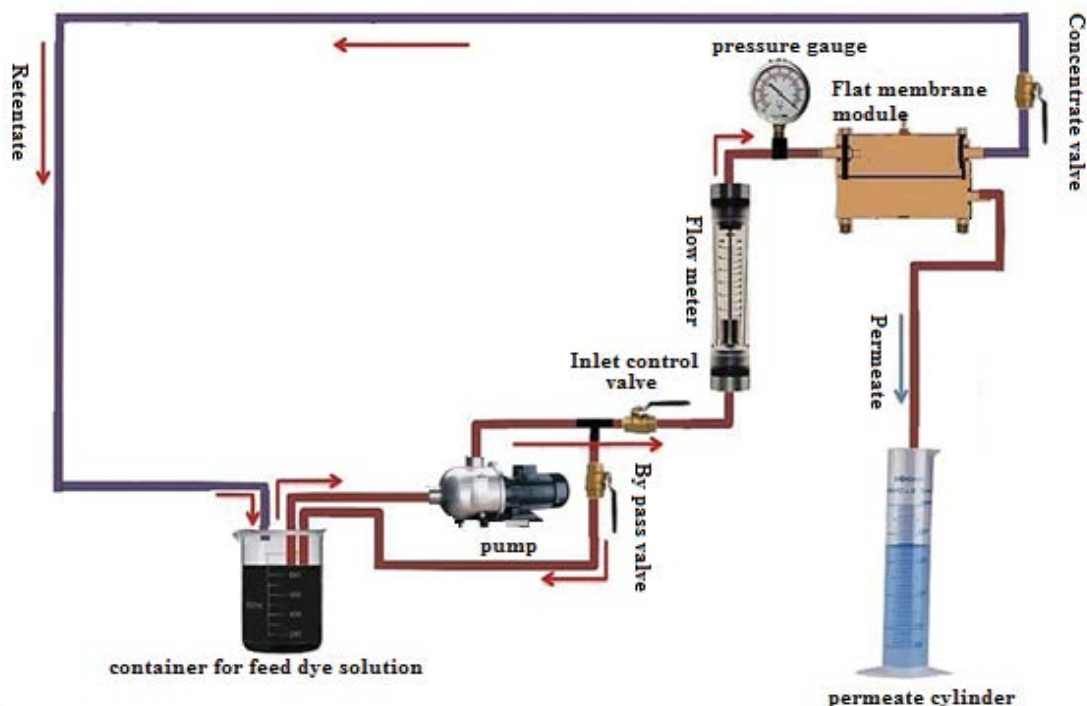
Fig. 1. Schematic diagram of the cross-flow filtration system.
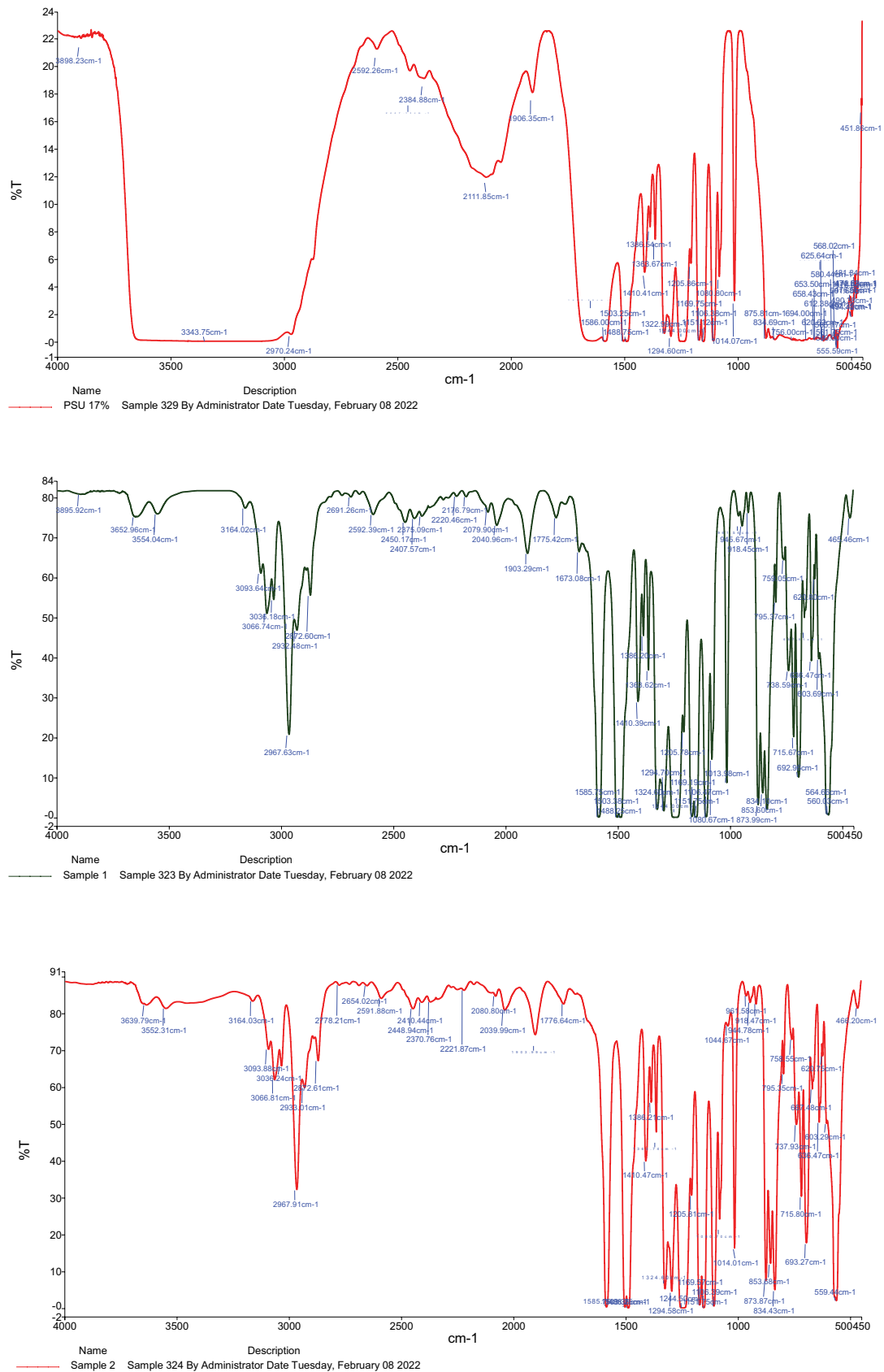
Fig. 2. Fourier-transform infrared spectroscopy (FTIR) of the PSU 17% (A) membrane, (B) after Malachite green experiment, and (C) membrane after Congo red experiment.

Name	The surface SEM images of membranes	The cross-sectional images of membranes
Mp3 = PSU 17%		
Mp2 = PSU 15%		
Mp1 = PSU 13%		
Ms3 = PES 17%		
Ms2 = PES 15%		
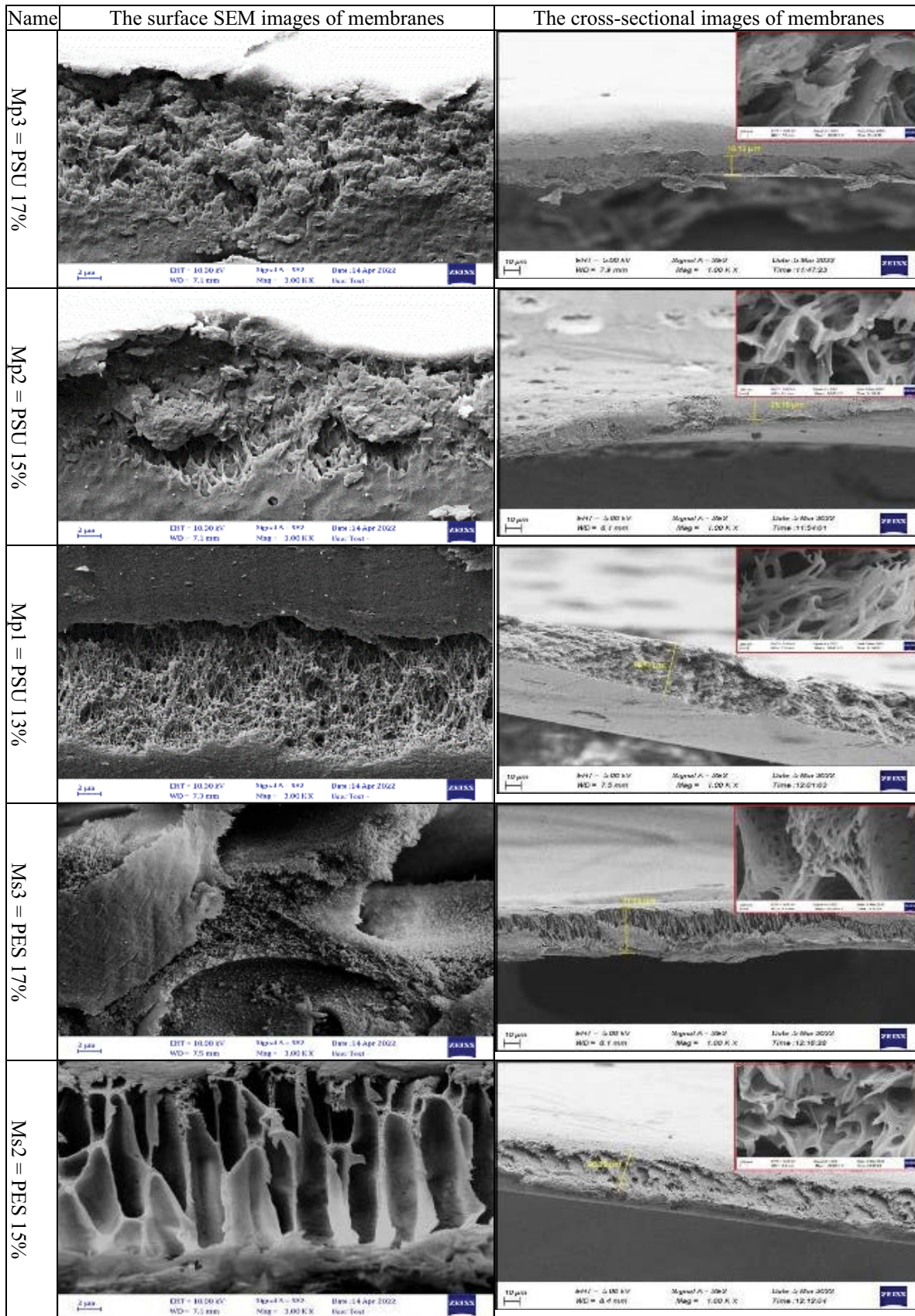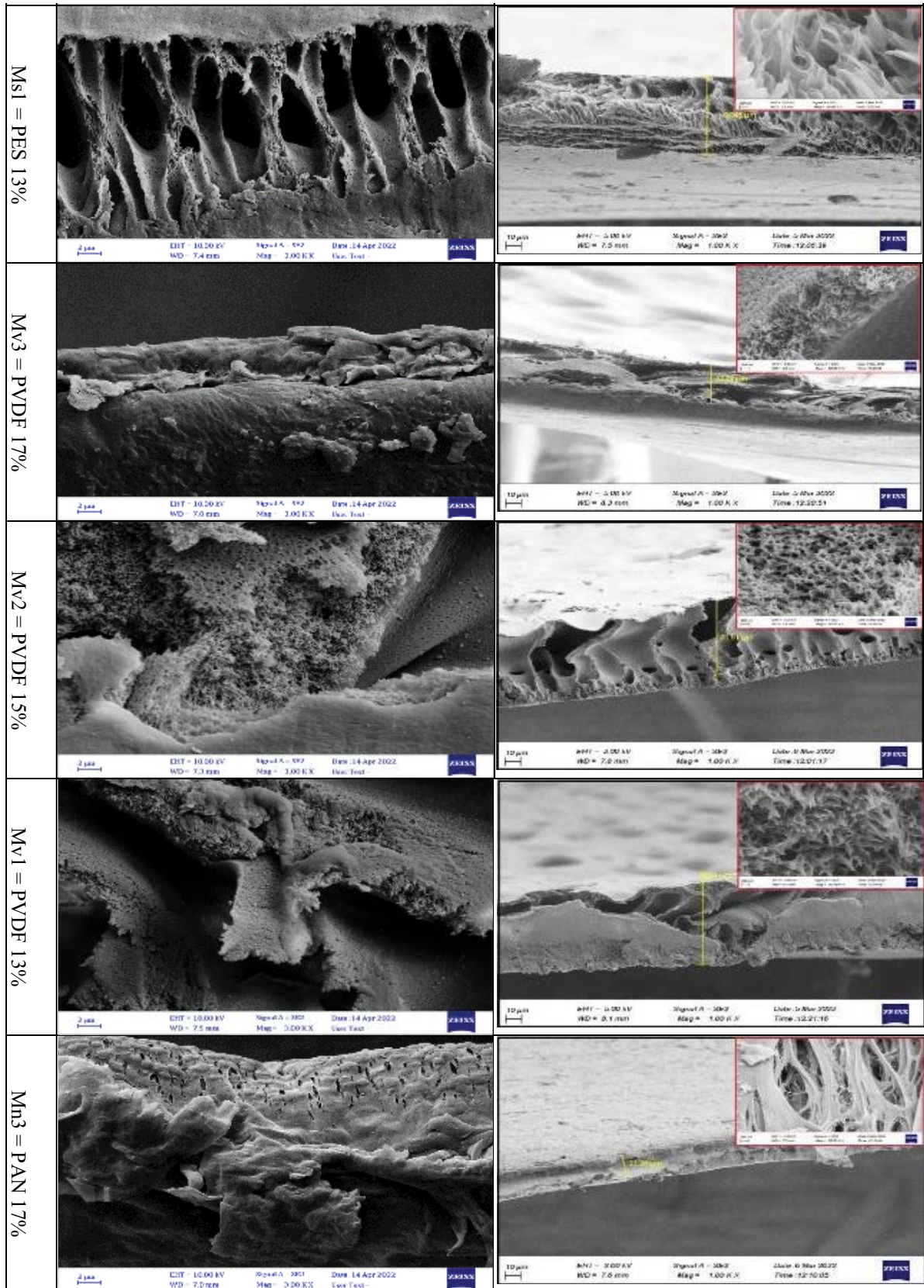
Fig. 3.   Continued

Fig. 3. Continued
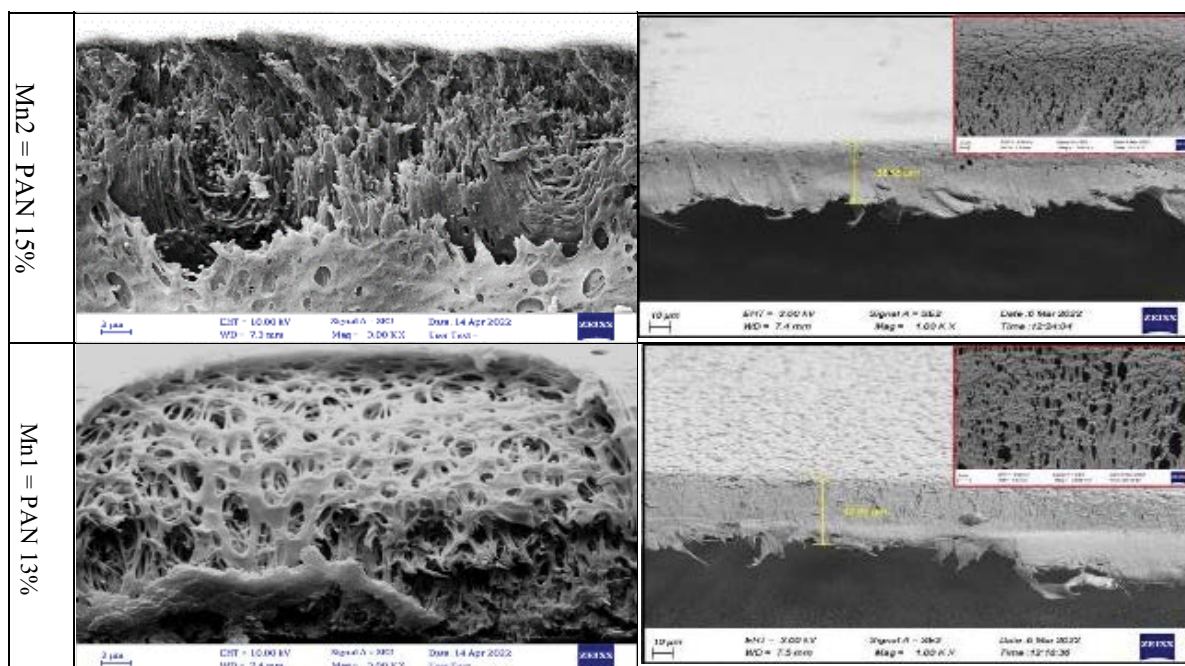
Fig. 3. SEM images of surface structure and cross-section morphology of PSU, PES, PAN and PVDF membranes prepared at 13%, 15%, and 17% concentrations.

of the PAN membrane is low in the concentration of 15%, the skin layers become less dense, and the porous becomes more dominant. In comparison, the PAN 13% membrane indicates that the microvoids increased significantly, and the top layers became a little permeable. This explains why PAN membranes made from low-concentration materials have a high penetration capacity.

The quantity of voids and large spaces reduces as the casting polymer concentration increases [52]. This narrowing and reduction in membrane pore number can be linked to a thickening of the membrane skin layer [52]. When the concentration of a solution rises, the amount of polymer in the membrane–bath contact rises, resulting in a decrease in solvent–nonsolvent exchange. The thickness of the resultant membranes increases as the PAN concentration increases, as shown in Fig. 3, which is consistent with prior findings [50,52].

Fig. 4 shows the SEM images of the PSU 17% membranes fouling after the dye removal experiments for Malachite green and Congo red dyes. Various morphological changes were observed, including an increase in the size and quantity of finger-like structures for both kinds of dyes. The lower and smaller finger-like pores were observed after the Malachite green experiment compared to the Congo red one. This may be attributed to operating conditions such as applied pressure and dye concentration at 100 ppm, in addition to the high molecular weights of dyes.

3.1.3. Atomic force microscopy images

The membranes' surface morphology is measured using the surface or average roughness (R_a), and root means square (R_q) using atomic force microscopy (AFM), as shown in Table 2. The surface roughness of the membrane increases with decreasing concentration of polymers. It can be noticed from Fig. 5 that the AFM images revealed that a 13% concentration of membranes showed a surface that was covered with valley or mountainous-like peaks compared with 15% and 17% of membranes that did not show such structure.

In general, the roughness parameters slightly decreased with increasing the polymer concentration in the casting solution. The average roughness of the membranes decreased from 9.06 nm (the PSU 13% membrane) to 8.567 nm (the PSU 15% membrane) and 8.017 nm (the PSU 17% membrane). On the other hand, the surface of the PES 17% membrane was even and regular in texture; additionally, there is not as much "valley"-like structure as depicted in 3D images. Compared with 15% and 13% PES membranes, nodules in various shapes were seen on the top surface, shown in Fig. 5. Surface roughness was significantly reduced by the PES polymer added to the membrane casting solution, going from 5.075 nm for the PES 13% membrane to 4.831 nm for the PES 15% membrane.

Based on the 3D images in Fig. 5, it is obvious that all the PAN membranes have ridge and valley structures. However, the 17% PAN membrane has some smooth surfaces. The 17% PAN membrane showed a considerable enhancement in the surface roughness (about 3.385 nm) compared to that of the PAN 15% membrane (about 5.033 nm) and the PAN 13% membrane (about 7.957 nm), as reported in Table 2.

It is noticed that the PVDF 13% membrane has much higher surface roughness than that of the PVDF 15% membrane at 27.15 and 9.479 nm, respectively. On the contrary, the surface roughness was significantly reduced to 6.230 nm for the 17% PVDF. From AFM results, it has been noted that PVDF membranes are rougher than other membranes. According to Rajesh et al. [53], a change in the membrane
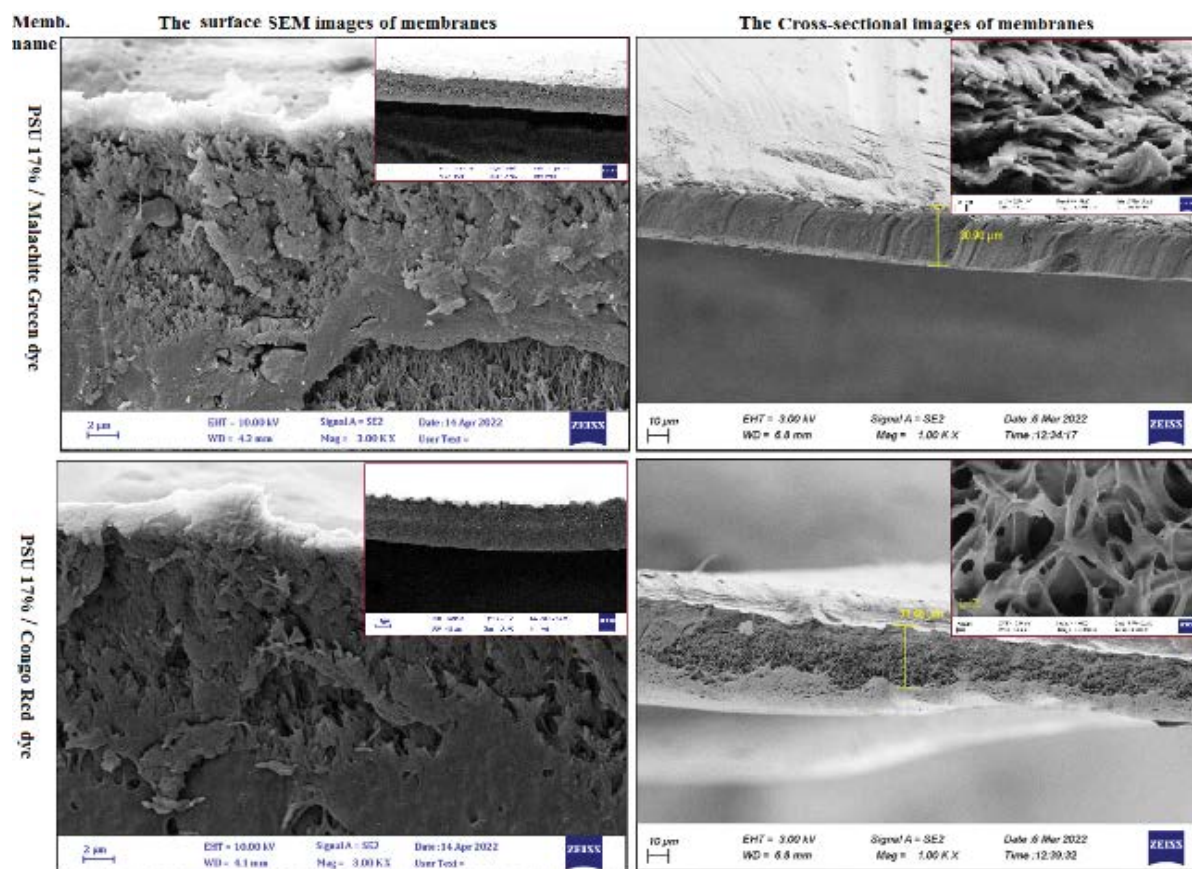
Fig. 4. SEM images of surface structure and cross-section morphology of (PSU 17%) membranes.

Table 2
Profile roughness parameters and porosity of prepared membranes

Membrane name	Porosity (%)	Average roughness, R_a (nm)	Root mean square roughness, Rrms (nm)
PSU 13%	54	9.06	31.24
PSU 15%	44	8.567	10.59
PSU 17%	38	8.017	10.42
PES 13%	56	5.075	6.323
PES 15%	50	4.831	6.081
PES 17%	44	3.146	5.558
PAN 13%	62	7.957	8.045
PAN 15%	60	5.033	5.700
PAN 17%	52	3.385	4.202
PVDF 13%	63	27.15	43.62
PVDF 15%	55	9.479	11.21
PVDF 17%	48	6.230	7.744

surface's mean roughness (R_a) corresponded to a change in pore size. Hong and He [54] reached concluded that the pore diameter might be determined by the solvent and coagulation bath (water) exchange rate during membrane formation.

Surface roughness is one of the most efficient factors in increasing the antifouling ability of membranes. Consequently, smoother membranes have better fouling resistance [55]. The results refer to the tendency to increase the concentration of polymers to 17 wt.%, leading to improve antifouling membrane performance due to the lower surface roughness compared to the membranes with concentrations of 13 and 15 wt.%. Sulfonated polymers were considered to be significantly more fouling resistant [56].
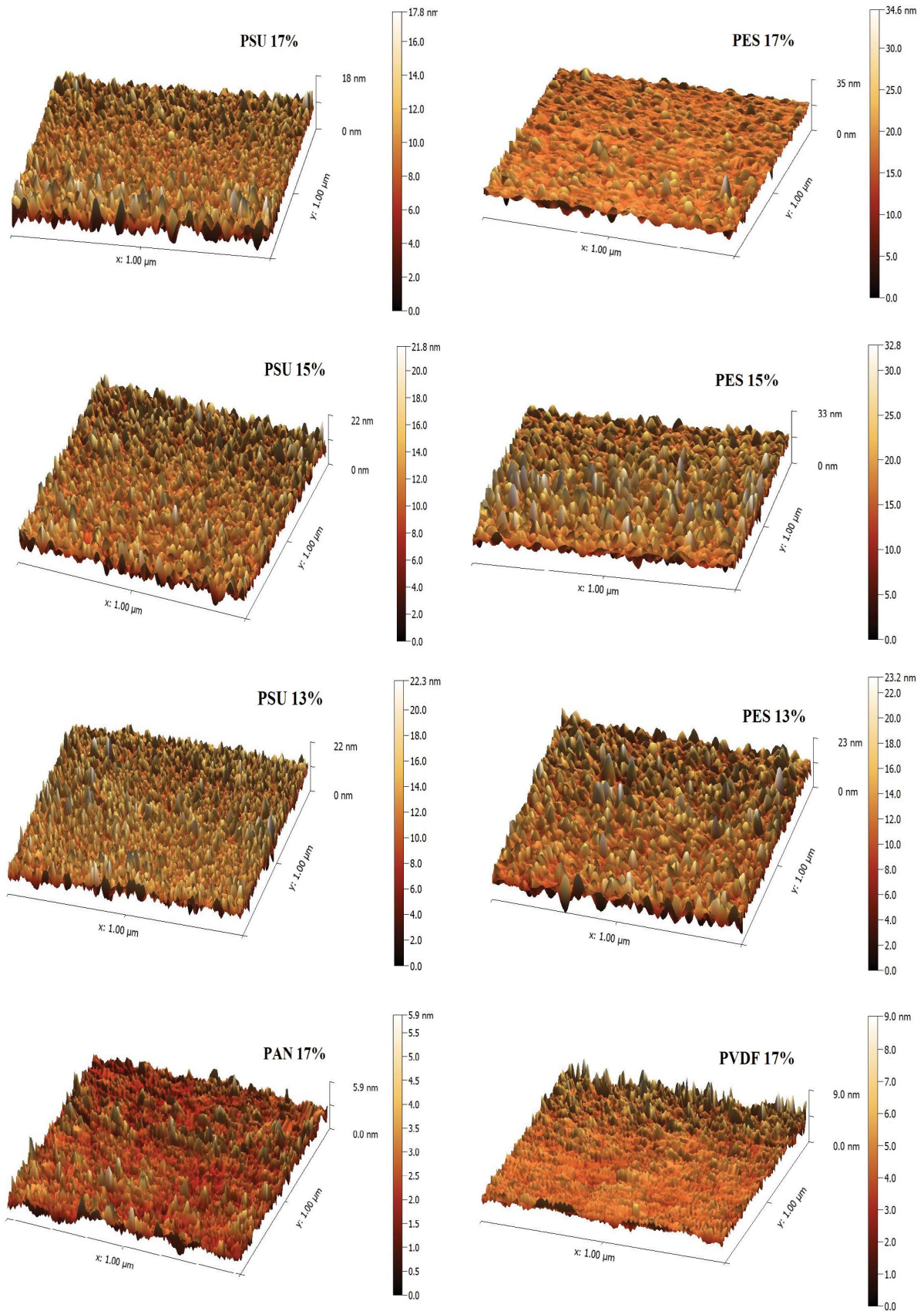
Fig. 5. Ctoninued
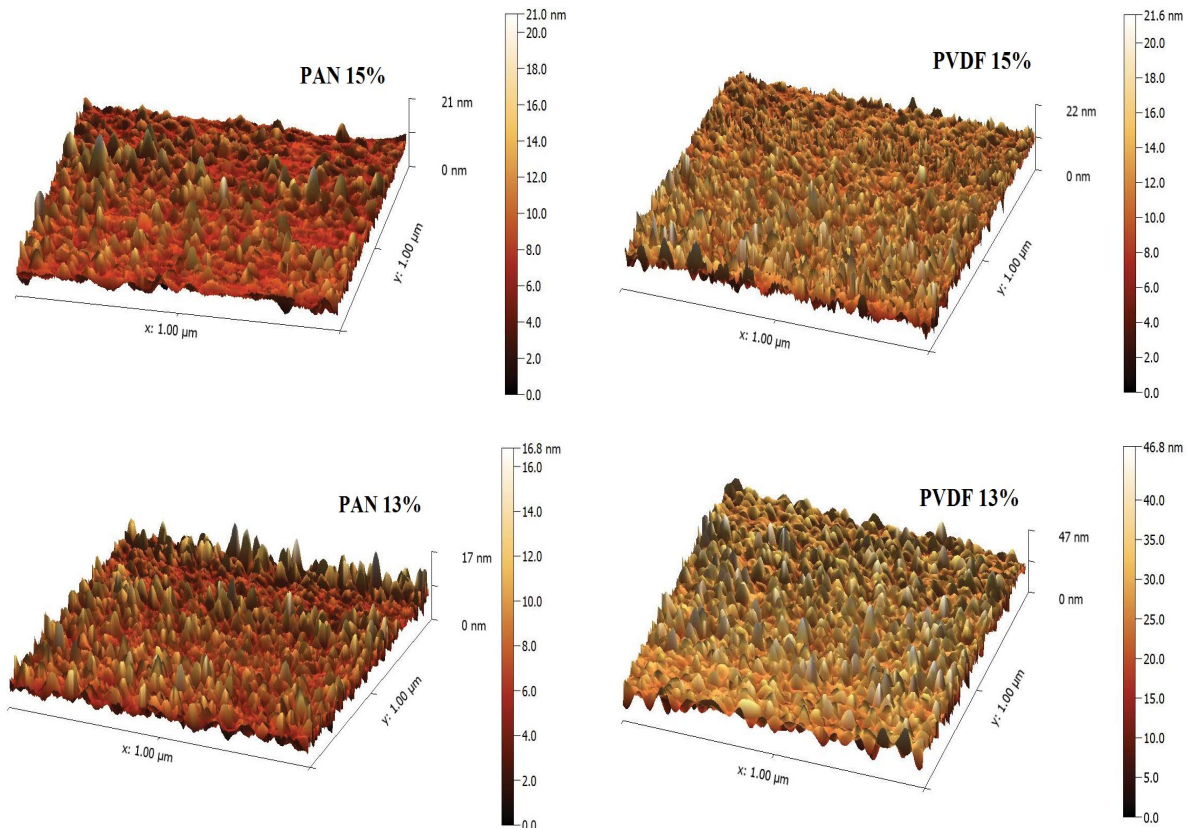
Fig. 5. 3D images of atomic force microscopy (AFM) of membranes.
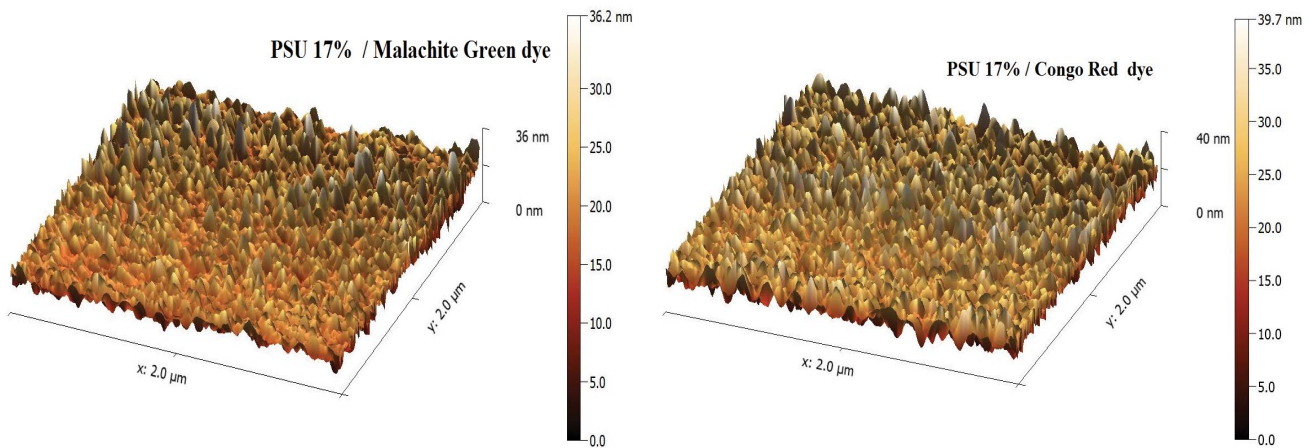
Fig. 6. AFM 3D images of PSU 17% membranes after antifouling performance.

However, after the antifouling performance of the membranes, the decrease in surface roughness in the PSU 17% membrane was due to the accumulation of foulants on the surface. The roughness decrease in the PSU 17% membrane after the dye removal experiment (Fig. 6) corresponds directly to the aggregation of dyes on the membrane surface. It is commonly known that foulants typically build up in the valley area, decreasing surface roughness [57–59].

3.1.4. Porosity

The porosities of all prepared membranes are reported in Table 2. Each membrane sample (6 cm²) was weighed using a digital weight balance, recorded as the wet and dry weights, and calculated using the gravimetric method by Eq. (1). The results displayed that increasing the concentration of polymers reduced the porosity of the membranes. This could be explained by the fact that polymer

concentrations increased the density of the membranes. It can be seen that the PSU 17% membrane recorded the lowest porosity at 38%, while the highest porosity at 63% for the PVDF 13% membrane.

3.2. Performance test

3.2.1. Effect of polymer concentration

Fig. 7 shows that the 13% PSU membrane was a circumstance in which the water flux increased quickly from 23.99 L/m²·h at 2 bar to 299.76 L/m²·h at 7 bar, while the rejection decreased from 91.91% to 73.72%. The water flux in the PSU 15% rose steadily from 17.61 L/m²·h at 2 bar to 59.52 L/m²·h at 7 bar, but the dye rejection decreased from 97.39% to 88.54%. However, when the concentration of PSU increased to 17%, the rejection declined slowly from 98.04% to 93.02% at 2 and 7 bar, respectively. Moreover, the water flux was recorded at 7.42 L/m²·h at 2 bar and 26.16 L/m²·h at 7 bar. It can be considered that PSU 17% membrane is the optimal membrane in terms of dye rejection

compared with other polymeric membranes. This may be ascribed to the smaller pore diameter of the PSU 17% membrane; therefore, the dye molecules are prevented from passing through the membrane. Surface porosity and pore size significantly reduced the PSU membrane fouling phenomenon [60,61].

It can be seen from Fig. 8 that increasing the concentration of PES resulted in improving dye removal while a decrease in water flux was reported. As in the PES 17% membrane, the dye removal was in the range of 97.44% and 86.78%, and the water flux changed moderately from 7.58 to 39.06 L/m²·h in 2 and 7 bar, respectively. In contrast, the water flux in the PES 13% membrane increased steeply from 42.64 L/m²·h in 2 bar to 613.12 L/m²·h in 7 bar, while the dye rejection fell from 91.51% to 70.55% at the same pressures. This may be credited increased in porosity (Table 2) and pore density.

The membrane performance for the PAN membranes in terms of water flux and rejection is illustrated in Fig. 9. It was observed that the PAN 13% membrane
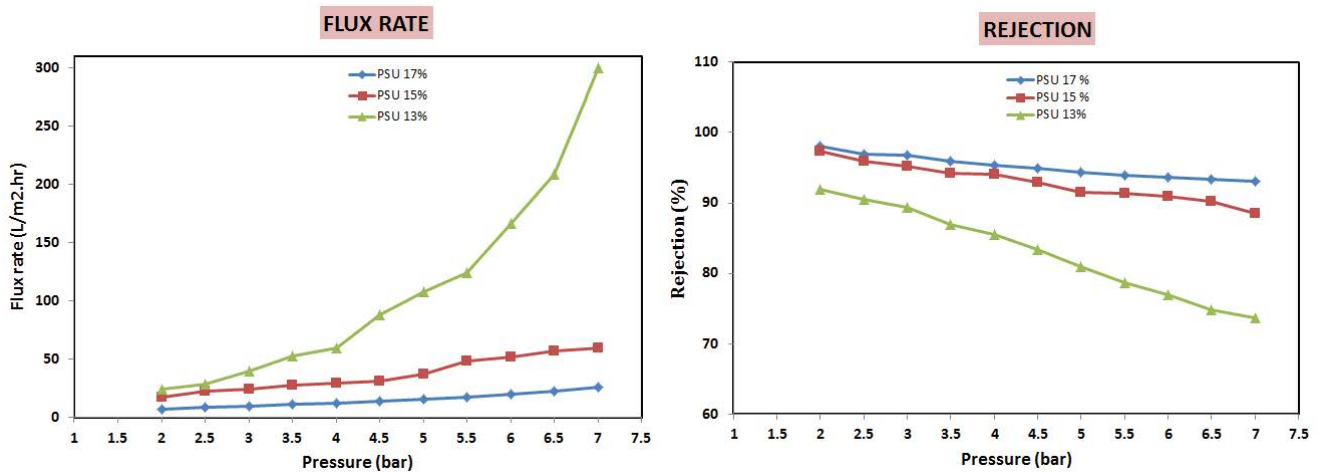
Fig. 7. Dye rejection and water flux for PSU membranes in Malachite green dye under operation conditions of 2–7 bar and 25°C.
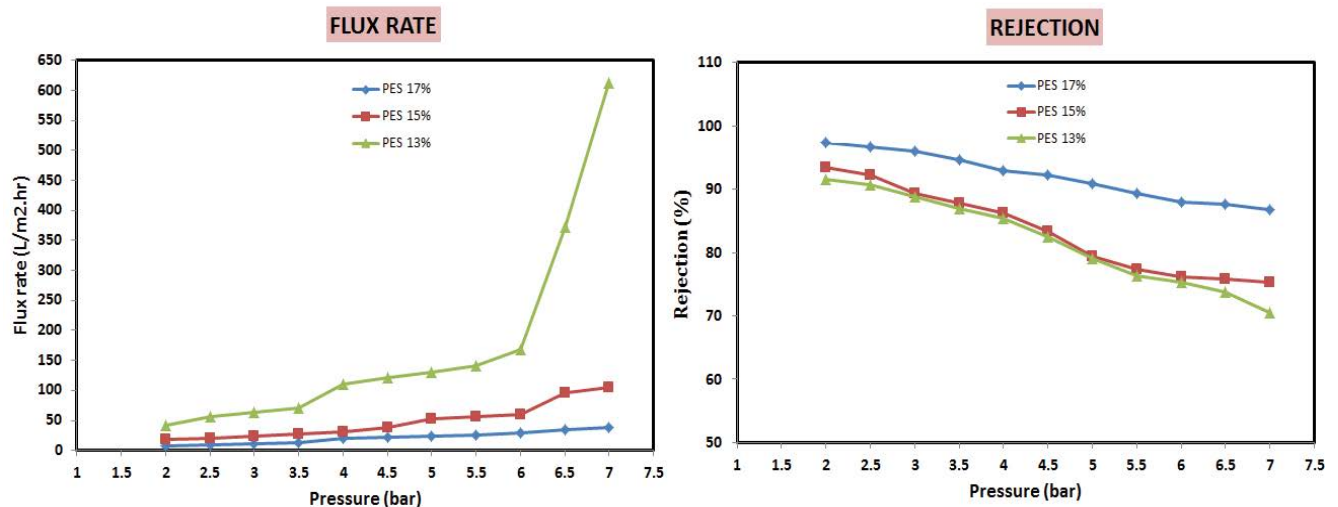
Fig. 8. Dye rejection and water flux for PES membranes in Malachite green dye under operation conditions of 2–7 bar and 25°C.

had a water flux of 45.35 L/m²·h, which is twice higher than that of the PAN 15% membrane and three times higher than that of the PAN 17% membrane at 2 bar. The water flux at 7 bar jumped sharply to 571.43 and 357.14 L/m²·h in PAN 13% and PAN 15%, respectively. As explained previously, the higher water flux in the PAN 13% membrane can be correlated to the increase in pore size. The increased porosity has facilitated the passage of the aqueous solution molecules through the membranes. The increased water flux is usually attributed to the increase in pore sizes [62]. Further, the dye rejection of the PAN 13% membrane was found to be 90.95% at 2 bar, whereas in the case of PAN 15% and PAN 17% membranes, the rejection was 93.47% and 95.07%, respectively. In 7 bar, dye removal for the PAN 13% membrane fell quickly to 58.44% compared with 77.84% for the PAN 15% membrane and 79.87% for the PAN 17% membrane.

Pure water flux and dye rejection results for the PVDF membranes are presented in Fig. 10. The membrane structure (SEM, AFM, and FTIR) and flux performance are compatible. Pore size and total pore count on the membrane surface directly correlate with water flux. The decrease of concentration PVDF from 17% to 15% led to a substantially growing fluxing from 50 to 156.25 L/m²·h. Also, the water flux of PVDF 13% membrane rose from 7.80 to 189.39 L/m²·h at the same pressures (from 2 to 7 bar). As transmembrane pressure (TMP) rises, this action is correlated with an increase in membrane driving force. While the membrane resistance is constant and TMP grows, the mass transfer driving force that causes water to move through the membrane pores increases [63]. Fig. 10 summarizes the rejection performance of PVDF membranes. The rejection for all samples was not significantly changed, while the greatest rejection value was for the PVDF 17% membrane with 97.09% at 2 bar. This rejection was greater than the 95.48% recorded by the PVDF 15% membrane and that of the PVDF 13% membrane (91.51%). Consequently, the higher dye rejection by the PVDF 17% membrane was attributable to decreased pore size. On the other hand, when pressure increased, the rejection reduced steadily. PVDF 17%, PVDF 15%, and PVDF 13% membranes at 7 bar recorded the rejection of 82.36%, 79.25% and 74.27%,
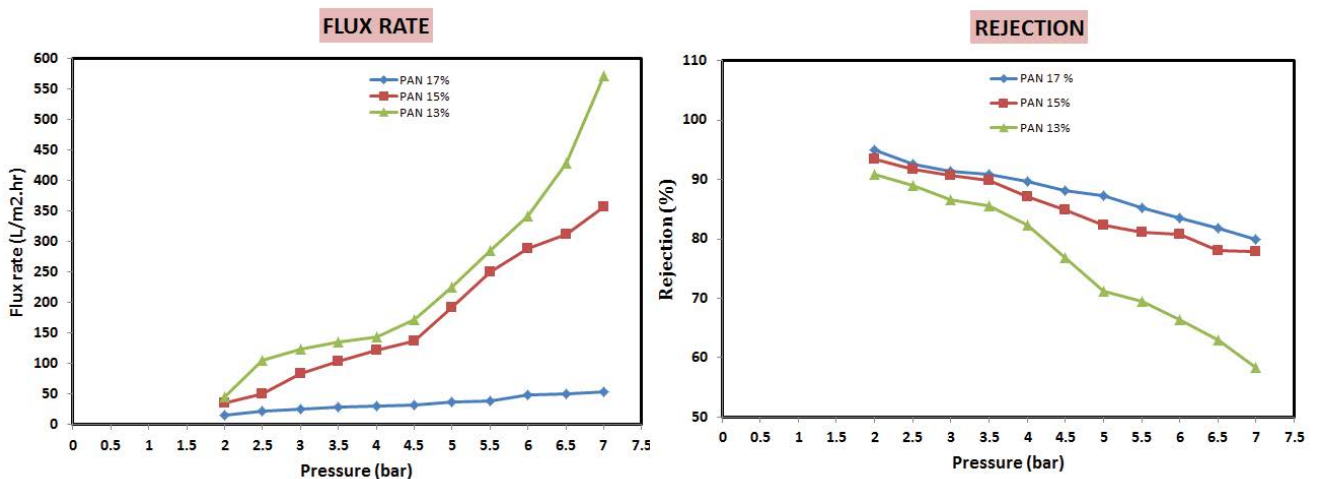
Fig. 9. Dye rejection and water flux for PAN membranes in Malachite green dye under operation conditions of 2–7 bar and 25°C.
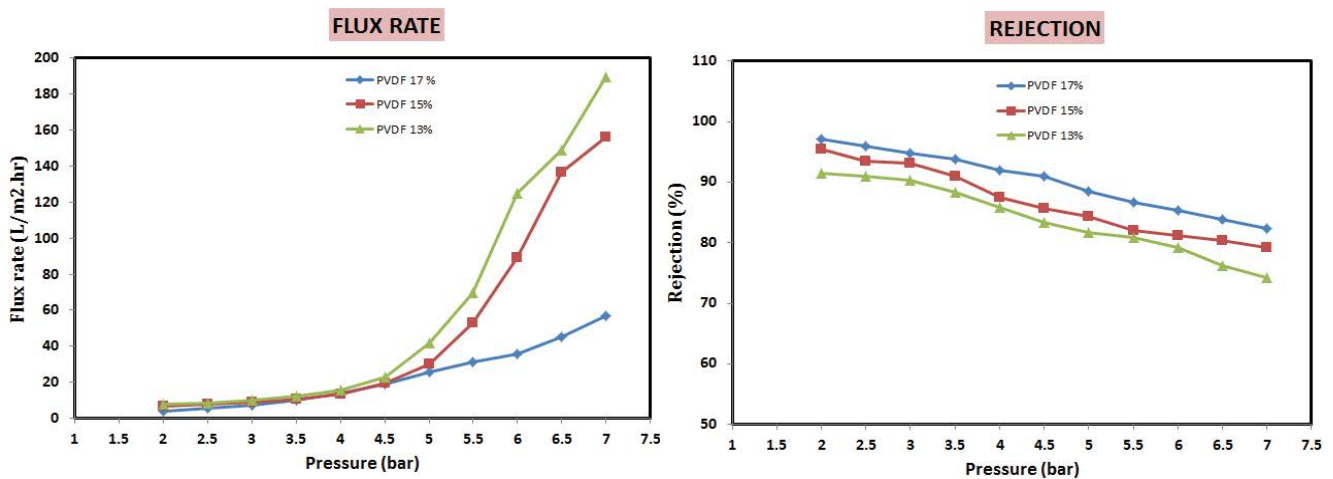
Fig. 10. Dye rejection and water flux for PVDF membranes in Malachite green dye under operation conditions of 2–7 bar and 25°C.

respectively. As explained above, this may be caused by the membranes' greater pore sizes.

3.2.2. Effect of polymer type

Fig. 11 compares the performance (water flux and dye rejection) of the four polymeric membranes prepared at a concentration of 17% using 100 ppm Malachite green as feed solution. The results demonstrate that the calculated permeability of tests does not increase linearly with the operating pressure. It is shown that the water flux of the PVDF 17% membrane is the lowest at 2 bar, and at the same time, it is the highest at 7 bar. Additional loss of permeability at initial pressures could be caused by dye molecules obstructing pores. Membrane fouling is one of the most critical challenges faced in the membrane separation processes that affect the performance of membrane filtration in terms of fluid separation and usage lifetime [64]. In Fig. 11, dye rejection is also shown against operating pressure. For four

polymer membranes at a concentration of 17%, increasing the pressure causes a decrease in solute rejection. All membranes recorded good rejection of Malachite green dye, but the highest removal was for the PSU 17% membrane at 98.04% at 2 bar and 93.02% at 7 bar.

As a result, the four polymer membranes with a percentage of 17% gave an excellent rejection rate for the Malachite green dye. These membranes were also tested by removing another dye (i.e., Congo red), and the permeate and rejection were excellent, as illustrated in Fig. 12. The PSU 17% membrane recorded the best rejection rate, in the range of 99.59% and 98.59% between 2 and 7 bar. The prepared membranes performed better in removing Congo red than Malachite green. In this work, the behavior of membranes for the removal of dyes with positive and negative charges can be explained by taking into account the rejection's two-step process [65]. The first step comes before the dyes are absorbed onto the membrane surface. Negatively charged dyes are absorbed less on the surface
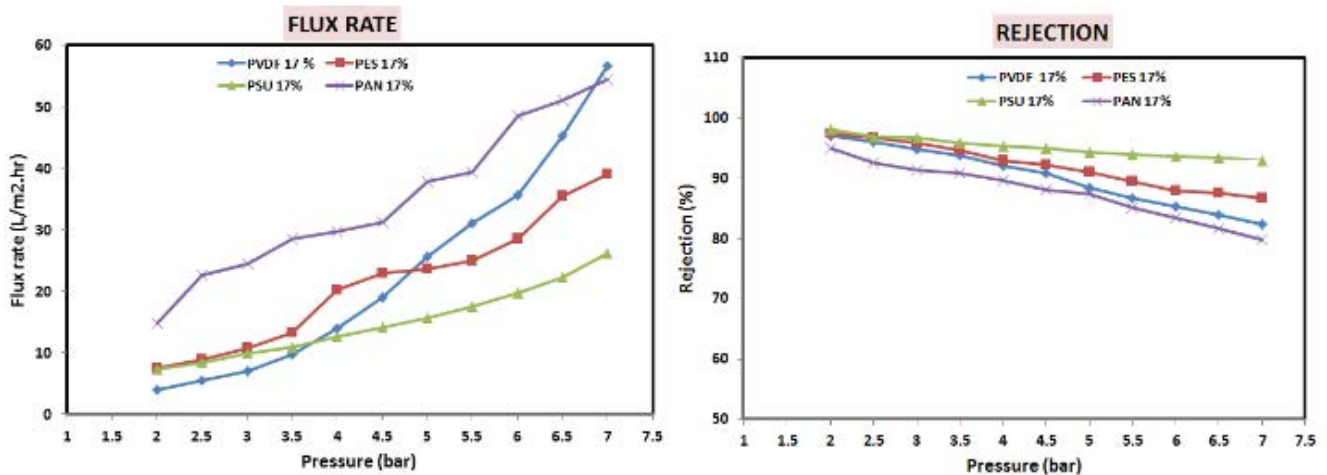
Fig. 11. Rejection and water flux of Malachite green dye vs. operating pressures 2–7 bar and 25°C by PSU, PES, PAN, and PVDF membranes at a concentration of 17%.
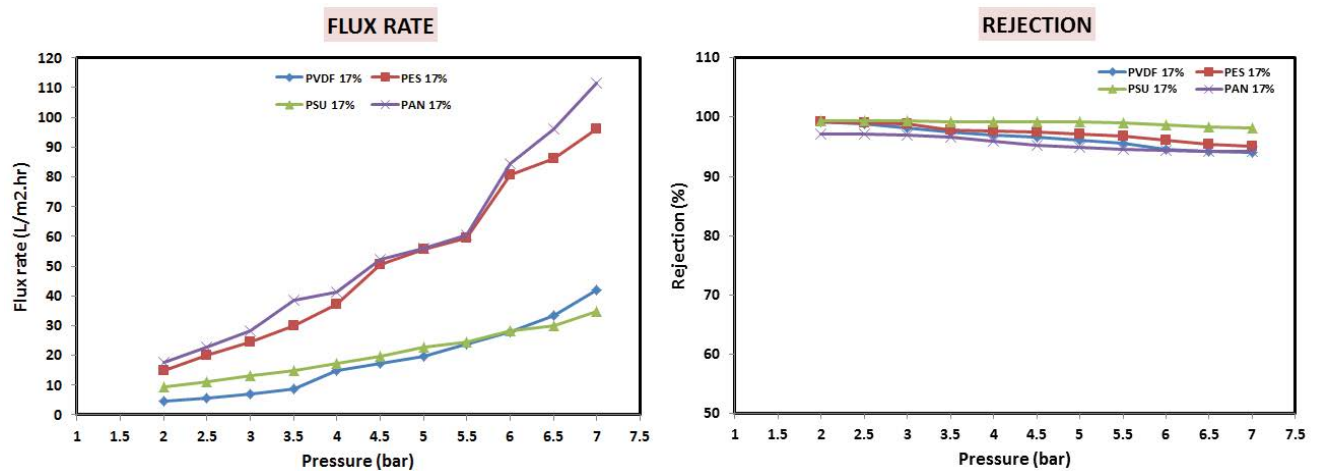
Fig. 12. Rejection and water flux of Congo red dye vs. operating pressures 2–7 bar and 25°C by PSU, PES, PAN, and PVDF membranes at a concentration of 17%.

of the membranes due to the repulsive force, and the repulsion that already exists enhances the effectiveness of membrane removal. In the second-stage, following the adsorption of dyes on membranes, the present interactions and pore size play a significant role in the removal of dyes, and increasing the interactions will improve the removal of dyes. As a result of the repulsive force on the membrane surface, dyes with negative charges have the highest rejection rate. Due to the high density of negative charges in Congo red dye, the removal % was the highest. In comparison, Malachite green dye had the lowest removal due to its positive charge and electrostatic adsorption on the membrane. However, it should also be noted that increased concentration polarization caused by higher pressure may cause a reduction in dye rejection [66]. Because dye rejections are starting to decline, it may be inferred that the results of the current investigation demonstrated that pressure had a favorable but not very substantial impact on dye rejection.

A thorough comparison of membrane separation performance with other reported/published data is shown in Table 3 to highlight the novelty of this work. This comparison was made using information from the recently published literature and was based on permeation water flux and dye rejection rate membrane applications. It is clear from Table 3 that the operating parameters stated in Section 2.3 apply to the membranes in the current experiment. The membranes are prepared with adequate water flux permeability and better dye rejection.

4. Conclusion

In summary, the reported study highlighted the various ultrafiltration membranes prepared by the phase inversion technique to remove Malachite green and Congo red dyes. Tests on these membranes' morphology and characterization were conducted. Increasing polymer concentration to 17% was shown to have a positive result on membranes by such effects as enhanced porosity, surface roughness, and structure of membranes. The SEM imaging revealed that the morphology of the 15% and 13% UF membranes have a porous and asymmetric structure, while the 17% UF membranes have a dense structure. The AFM images demonstrated that the 17% UF membranes significantly reduced the average roughness, leading to a low membrane porosity level. The increase of concentration to 17% also improved the dye rejection. This was most evident in the instance of Congo red dye. In contrast, membranes with 13% content appeared to have less dye rejection because adding polymer reduced the membranes' porosity. The results showed that the optimum operating pressure was 2 bar. It was found that above 95% rejection of both dyes was achieved with pristine membranes with a concentration of 17%. Also, it can be seen that the PSU 17% membrane achieved the highest removal for Malachite green and Congo red dyes at 98.04% and 99.42% and recorded acceptable flux rates at 8.06 and 10.96 L/m²·h at 2 bar, respectively. The permeability and rejection performance suggest that the PSU 17% membrane is more potent and promising for treating of dye-polluted wastewater.

Table 3
Demonstrates the comparison of this work with the recently published membranes

Membrane materials and content (wt.%)	Dye type	Operating pressure (bar)	Permeate (L/m²·h)	Rejection (%)	References
Polyvinylidene fluoride (PVDF) (20)	Acid yellow 23	4	180	90	[67]
Polysulfone (PSU) (18)	Crystal violet	5	10	100	[68]
Polyethersulfone (PES) (20)	Direct red 23;	5	19.1	98.94	[69]
	Congo red;		19.1	98.4	
	Direct red 243		19.9	99.33	
Polyphenylsulfone (PPSU) (20)	Drupel Black NT	1	22	88	[70]
Polyethersulfone (PES) (21)	Acid black	3	12	88	[71]
	Rose bengal		10	86	
Polyethersulfone (PES) (20)	Congo red	1	4	90	[72]
	Reactive black		4.5	87	
Polyethersulfone (PES) (17)	Bovine serum albumin (BSA)	2	100	85	[73]
Polysulfone (PSU) (18)	BSA protein;	1.5	224.5	66.02	[74]
	Rhodamine 6G		224.5	45.19	
Polysulfone (PSU) (17)	Malachite green	2	7.42	98	This study
	Congo red		9.33	99.40	
Polyethersulfone (PES) (17)	Malachite green	2	7.58	97.44	This study
	Congo red		15.06	99.19	
Polyvinylidene fluoride (PVDF) (17)	Malachite green	2	4.02	97.09	This study
	Congo red		4.46	99.13	
Polyacrylonitrile (PAN) (17)	Malachite green	2	14.86	95.07	This study
	Congo red		17.66	97.22	

References

[1] H. Zollinger, Color Chemistry: Syntheses, Properties, and Applications of Organic Dyes and Pigments, John Wiley & Sons, Weinheim, Germany, 2003.

[2] K. Kümmerer, The presence of pharmaceuticals in the environment due to human use–present knowledge and future challenges, J. Environ. Manage., 90 (2009) 2354–2366.

[3] U. Baig, M.K. Uddin, M.A. Gondal, Removal of hazardous azo dye from water using synthetic nano adsorbent: facile synthesis, characterization, adsorption, regeneration and design of experiments, Colloids Surf., A, 584 (2020) 124031, doi: 10.1016/j.colsurfa.2019.124031.

[4] H.S. Rai, M.S. Bhattacharyya, J. Singh, T.K. Bansal, P. Vats, U.C. Banerjee, Removal of dyes from the effluent of textile and dyestuff manufacturing industry: a review of emerging techniques with reference to biological treatment, Crit. Rev. Env. Sci. Technol., 35 (2005) 219–238.

[5] N.H. Torres, B.S. Souza, L.F.R. Ferreira, A.S. Lima, G.N. dos Santos, E.B. Cavalcanti, Real textile effluents treatment using coagulation/flocculation followed by electrochemical oxidation process and ecotoxicological assessment, Chemosphere, 236 (2019) 124309, doi: 10.1016/j.chemosphere.2019.07.040.

[6] Y.A. Oktem, B. Yuzer, M.I. Aydin, H.E. Okten, S. Meric, H. Selcuk, Chloride or sulfate? Consequences for ozonation of textile wastewater, J. Environ. Manage., 247 (2019) 749–755.

[7] E. Gregušková, K. Mičieta, Phytoindication of the ecogenotoxic effects of vehicle emissions using pollen abortion test with native flora, Pol. J. Environ. Stud., 22 (2013) 1069–1076.

[8] K.B. Daij, S. Bellebia, Z. Benghalez, Comparative experimental study on the COD removal in aqueous solution of pesticides by the electrocoagulation process using monopolar iron electrodes, Chem. Int., 3 (2017) 420–427.

[9] M.A. Jamal, M. Muneer, M. Iqbal, Photo-degradation of monoazo dye blue 13 using advanced oxidation process, Chem. Int., 1 (2015) 12–16.

[10] S. Sugashini, T. Gomathi, R.A. Devi, P.N. Sudha, K. Rambabu, F. Banat, Nanochitosan/carboxymethyl cellulose/TiO$_2$ bio-composite for visible-light-induced photocatalytic degradation of Crystal violet dye, Environ. Res., 204 (2022) 112047, doi: 10.1016/j.envres.2021.112047.

[11] A. Chham, E.H. Khouya, M. Oumam, A. Abourriche, S. Gmouh, M. Larzek, S. Mansouri, N. Elhammoudi, N. Hanafi, H. Hannache, The use of insoluble mater of Moroccan oil shale for removal of dyes from aqueous solution, Chem. Int., 4 (2018) 67–77.

[12] S. Benkhaya, S. M'rabet, A. El Harfi, A review on classifications, recent synthesis and applications of textile dyes, Inorg. Chem. Commun., 115 (2020) 107891, doi: 10.1016/j.inoche.2020.107891.

[13] M. Breida, S.A. Younssi, A. Bouazizi, B. Achiou, M. Ouammou, M. El Rhazi, Nitrate removal from aqueous solutions by γ-Al$_2$O$_3$ ultrafiltration membranes, Heliyon, 4 (2018) e00498, doi: 10.1016/j.heliyon.2017.e00498.

[14] S. Benkhaya, B. Achiou, M. Ouammou, J. Bennazha, S.A. Younssi, S. M'rabet, A. El Harfia, Preparation of low-cost composite membrane made of polysulfone/polyetherimide ultrafiltration layer and ceramic pozzolan support for dyes removal, Mater. Today Commun., 19 (2019) 212–219.

[15] C.F. Couto, L.C. Lange, M.C.S. Amaral, A critical review on membrane separation processes applied to remove pharmaceutically active compounds from water and wastewater, J. Water Process Eng., 26 (2018) 156–175.

[16] R. Castro-Muñoz, G. Boczkaj, E. Gontarek, A. Cassano, V. Fíla, Membrane technologies assisting plant-based and agro-food by-products processing: a comprehensive review, Trends Food Sci. Technol., 95 (2020) 219–232.

[17] X. Li, H. Shan, W. Zhang, B. Li, 3D printed robust superhydrophilic and underwater superoleophobic composite membrane for high efficient oil/water separation, Sep. Purif. Technol., 237 (2020) 116324, doi: 10.1016/j.seppur.2019.116324.

[18] H. Saleem, L. Trabzon, A. Kilic, S.J. Zaidi, Recent advances in nanofibrous membranes: production and applications in water

[19] C.A. Scholes, Hydrogen cyanide recovery by membrane gas separation, Chem. Eng. J., 386 (2020) 124049, doi: 10.1016/j.cej.2020.124049.

[20] P.A. Sosa-Fernandez, J.W. Post, F.A.M. Leermakers, H.H.M. Rijnaarts, H. Bruning, Removal of divalent ions from viscous polymer-flooding produced water and seawater via electrodialysis, J. Membr. Sci., 589 (2019) 117251, doi: 10.1016/j.memsci.2019.117251.

[21] N. Oussama, H. Bouabdesselam, N. Ghaffour, L. Abdelkader, Characterization of seawater reverse osmosis fouled membranes from large scale commercial desalination plant, Chem. Int., 5 (2019) 158–167.

[22] E. Filloux, B. Teychene, A. Tazi-Pain, J.-P. Croue, Ultrafiltration of biologically treated domestic wastewater: how membrane properties influence performance, Sep. Purif. Technol., 134 (2014) 178–186.

[23] S.-H. Zhi, L.-S. Wan, Z.-K. Xu, Poly(vinylidene fluoride)/poly(acrylic acid)/calcium carbonate composite membranes via mineralization, J. Membr. Sci., 454 (2014) 144–154.

[24] Y. Ma, F. Shi, J. Ma, M. Wu, J. Zhang, C. Gao, Effect of PEG additive on the morphology and performance of polysulfone ultrafiltration membranes, Desalination, 272 (2011) 51–58.

[25] K. Nouzaki, M. Nagata, J. Arai, Y. Idemoto, N. Koura, H. Yanagishita, H. Negishi, D. Kitamoto, T. Ikegami, K. Haraya, Preparation of polyacrylonitrile ultrafiltration membranes for wastewater treatment, Desalination, 144 (2002) 53–59.

[26] R. Krishnamoorthy, V. Sagadevan, Polyethylene glycol and iron oxide nanoparticles blended polyethersulfone ultrafiltration membrane for enhanced performance in dye removal studies, e-Polymers, 15 (2015) 151–159.

[27] A.L. Ahmad, A.A. Abdulkarim, B.S. Ooi, S. Ismail, Recent development in additives modifications of polyethersulfone membrane for flux enhancement, Chem. Eng. J., 223 (2013) 246–267.

[28] D.M. Al-Ani, F.H. Al-Ani, Q.F. Alsalhy, S.S. Ibrahim, Preparation and characterization of ultrafiltration membranes from PPSU-PES polymer blend for dye removal, Chem. Eng. Commun., 208 (2021) 41–59.

[29] M.H. Al-Furaiji, K.R. Kalash, M.A. Kadhom, Q.F. Alsalhy, Evaluation of polyethersulfone microfiltration membranes embedded with MCM-41 and SBA-15 particles for turbidity removal, Desal. Water Treat., 215 (2021) 50–59.

[30] K. Kalash, M. Kadhom, M. Al-Furaiji, Thin film nanocomposite membranes filled with MCM-41 and SBA-15 nanoparticles for brackish water desalination via reverse osmosis, Environ. Technol. Innovation, 20 (2020) 101101, doi: 10.1016/j.eti.2020.101101.

[31] S.S. Hussein, S.S. Ibrahim, M.A. Toma, Q.F. Alsalhy, E. Drioli, Novel chemical modification of polyvinyl chloride membrane by free radical graft copolymerization for direct contact membrane distillation (DCMD) application, J. Membr. Sci., 611 (2020) 118266, doi: 10.1016/j.memsci.2020.118266.

[32] S. Zinadini, A.A. Zinatizadeh, M. Rahimi, V. Vatanpour, H. Zangeneh, Preparation of a novel antifouling mixed matrix PES membrane by embedding graphene oxide nanoplates, J. Membr. Sci., 453 (2014) 292–301.

[33] M. Abedi, M. Sadeghi, M.P. Chenar, Improving antifouling performance of PAN hollow fiber membrane using surface modification method, J. Taiwan Inst. Chem. Eng., 55 (2015) 42–48.

[34] M. Abedi, M.P. Chenar, M. Sadeghi, Surface modification of PAN hollow fiber membrane by chemical reaction, Fibers Polym., 16 (2015) 788–793.

[35] M.R. Esfahani, J.L. Tyler, H.A. Stretz, M.J.M. Wells, Effects of a dual nanofiller, nano-TiO$_2$ and MWCNT, for polysulfone-based nanocomposite membranes for water purification, Desalination, 372 (2015) 47–56.

[36] K. Rambabu, S. Gokul, A.S. Russel, S. Akella, P. Babu, F. Banat, Lithium perchlorate modified nanoporous polyethersulfone membranes for improved dye rejection, Desal. Water Treat., 122 (2018) 146–157.

[37] C. Evangeline, V. Pragasam, K. Rambabu, S. Velu, P. Monash, G. Arthanareeswaran, F. Banat, Iron oxide modified polyethersulfone/cellulose acetate blend membrane for enhanced defluoridation application, Desal. Water Treat., 156 (2019) 177–188.

[38] N. Viart, D. Niznansky, J.L. Rehspringer, Structural evolution of a formamide modified sol—spectroscopic study, J. Sol-Gel Sci. Technol., 8 (1997) 183–187.

[39] X. Ma, N.-H. Lee, H.-J. Oh, J.-S. Hwang, S.-J. Kim, Preparation and characterization of silica/polyamide-imide nanocomposite thin films, Nanoscale Res. Lett., 5 (2010) 1846–1851.

[40] Z. Zhenxin, T. Matsuura, Discussions on the formation mechanism of surface pores in reverse osmosis, ultrafiltration, and microfiltration membranes prepared by phase inversion process, J. Colloid Interface Sci., 147 (1991) 307–315.

[41] Q.-Z. Zheng, P. Wang, Y.-N. Yang, Rheological and thermodynamic variation in polysulfone solution by PEG introduction and its effect on kinetics of membrane formation via phase-inversion process, J. Membr. Sci., 279 (2006) 230–237.

[42] J.-F. Blanco, J. Sublet, Q.T. Nguyen, P. Schaetzel, Formation and morphology studies of different polysulfones-based membranes made by wet phase inversion process, J. Membr. Sci., 283 (2006) 27–37.

[43] M.-J. Han, D. Bhattacharyya, Changes in morphology and transport characteristics of polysulfone membranes prepared by different demixing conditions, J. Membr. Sci., 98 (1995) 191–200.

[44] Z. Wang, J. Ma, Q. Liu, Pure sponge-like membranes bearing both high water permeability and high retention capacity, Desalination, 278 (2011) 141–149.

[45] V.P. Khare, A.R. Greenberg, J. Zartman, W.B. Krantz, P. Todd, Macrovoid growth during polymer membrane casting, Desalination, 145 (2002) 17–23.

[46] M. Pakizeh, S.A.A. Mansoori, M. Pourafshari Chenar, M. Namvar-Mahboub, Modification of PSf membrane nanostructure using different fabrication parameters and investigation of the CO_2 separation properties of PDMS-coated PSf composite membranes, Braz. J. Chem. Eng., 30 (2013) 345–354.

[47] S.S. Madaeni, A. Rahimpour, Effect of type of solvent and non-solvents on morphology and performance of polysulfone and polyethersulfone ultrafiltration membranes for milk concentration, Polym. Adv. Technol., 16 (2005) 717–724.

[48] C. Barth, M.C. Goncalves, A.T.N. Pires, J. Roeder, B.A. Wolf, Asymmetric polysulfone and polyethersulfone membranes: effects of thermodynamic conditions during formation on their performance, J. Membr. Sci., 169 (2000) 287–299.

[49] C. Barth, M.C. Goncalves, A.T.N. Pires, J. Roeder, B.A. Wolf, Fine structure of poly(vinylidene fluoride) membranes prepared by phase inversion from a water/N-methyl-2-pyrollidone/poly(vinylidene fluoride) system, J. Polym. Sci., Part B: Polym. Phys., 42 (2004) 830–842.

[50] M.G. Buonomenna, P. Macchi, M. Davoli, E. Drioli, Poly(vinylidene fluoride) membranes by phase inversion: the role the casting and coagulation conditions play in their morphology, crystalline structure and properties, Eur. Polym. J., 43 (2007) 1557–1572.

[51] Z. Zhang, Q. An, Y. Ji, J. Qian, C. Gao, Effect of zero shear viscosity of the casting solution on the morphology and permeability of polysulfone membrane prepared via the phase-inversion process, Desalination, 260 (2010) 43–50.

[52] S. Darvishmanesh, J.C. Jansen, F. Tasselli, E. Tocci, P. Luis, J. Degrève, E. Drioli, B. Van der Bruggen, Novel polyphenylsulfone membrane for potential use in solvent nanofiltration, J. Membr. Sci., 379 (2011) 60–68.

[53] S. Rajesh, P. Maheswari, S. Senthilkumar, A. Jayalakshmi, D. Mohan, Preparation and characterisation of poly (amide-imide) incorporated cellulose acetate membranes for polymer enhanced ultrafiltration of metal ions, Chem. Eng. J., 171 (2011) 33–44.

[54] J. Hong, Y. He, Polyvinylidene fluoride ultrafiltration membrane blended with nano-ZnO particle for photo-catalysis self-cleaning, Desalination, 332 (2014) 67–75.

[55] X. Cao, J. Ma, X. Shi, Z. Ren, Effect of TiO_2 nanoparticle size on the performance of PVDF membrane, Appl. Surf. Sci., 253 (2006) 2003–2010.

[56] A. Nabe, E. Staude, G. Belfort, Surface modification of polysulfone ultrafiltration membranes and fouling by BSA solutions, J. Membr. Sci., 133 (1997) 57–72.

[57] A. Idris, N.M. Zain, M.Y. Noordin, Synthesis, characterization and performance of asymmetric polyethersulfone (PES) ultrafiltration membranes with polyethylene glycol of different molecular weights as additives, Desalination, 207 (2007) 324–339.

[58] J. Lin, C.Y. Tang, C. Huang, Y.P. Tang, W. Ye, J. Li, J. Shen, R. Van den Broeck, J. Van Impe, A. Volodin, C, Van Haesendonck, A. Sotto, P. Luis, B. Van der Bruggena, A comprehensive physico-chemical characterization of superhydrophilic loose nanofiltration membranes, J. Membr. Sci., 501 (2016) 1–14.

[59] E.M. Vrijenhoek, S. Hong, M. Elimelech, Influence of membrane surface properties on initial rate of colloidal fouling of reverse osmosis and nanofiltration membranes, J. Membr. Sci., 188 (2001) 115–128.

[60] G. Nechifor, S.I. Voicu, A.C. Nechifor, S. Garea, Nanostructured hybrid membrane polysulfone-carbon nanotubes for hemodialysis, Desalination, 241 (2009) 342–348.

[61] N.A.A. Hamid, A.F. Ismail, T. Matsuura, A.W. Zularisam, W.J. Lau, E. Yuliwati, M.S. Abdullah, Morphological and separation performance study of polysulfone/titanium dioxide (PSF/TiO_2) ultrafiltration membranes for humic acid removal, Desalination, 273 (2011) 85–92.

[62] S. Majeed, D. Fierro, K. Buhr, J. Wind, B. Du, A. Boschetti-de-Fierro, V. Abetz, Multi-walled carbon nanotubes (MWCNTs) mixed polyacrylonitrile (PAN) ultrafiltration membranes, J. Membr. Sci., 403 (2012) 101–109.

[63] M.K. Purkait, S. DasGupta, S. De, Removal of dye from wastewater using micellar-enhanced ultrafiltration and recovery of surfactant, Sep. Purif. Technol., 37 (2004) 81–92.

[64] S. Zinadini, A.A. Zinatizadeh, M. Rahimi, V. Vatanpour, H. Zangeneh, M. Beygzadeh, Novel high flux antifouling nanofiltration membranes for dye removal containing carboxymethyl chitosan coated Fe_3O_4 nanoparticles, Desalination, 349 (2014) 145–154.

[65] M. Mahmoudian M.G. Kochameshki, The performance of polyethersulfone nanocomposite membrane in the removal of industrial dyes, Polymer (Guildf), 224 (2021) 123693, doi: 10.1016/j.polymer.2021.123693.

[66] I. Petrinić, N.P.R. Andersen, S. Šostar-Turk, A.M. Le Marechal, The removal of reactive dye printing compounds using nanofiltration, Dyes Pigm., 74 (2007) 512–518.

[67] A. Akbari, M. Hamadanian, V. Jabbari, A.Y. Lehi, M. Bojaran, Influence of PVDF concentration on the morphology, surface roughness, crystalline structure, and filtration separation properties of semicrystalline phase inversion polymeric membranes, Desal. Water Treat., 46 (2012) 96–106.

[68] M.R.S. Kebria, M. Jahanshahi, A. Rahimpour, SiO_2 modified polyethyleneimine-based nanofiltration membranes for dye removal from aqueous and organic solutions, Desalination, 367 (2015) 255–264.

[69] T. Tavangar, M. Karimi, M. Rezakazemi, K.R. Reddy, T.M. Aminabhavi, Textile waste, dyes/inorganic salts separation of cerium oxide-loaded loose nanofiltration polyethersulfone membranes, Chem. Eng. J., 385 (2020) 123787, doi: 10.1016/j.cej.2019.123787.

[70] M.Y. Ghadhban, H. Shaker Majdi, K.T. Rashid, Q.F. Alsalhy, D. Shanthana Lakshmi, I.K. Salih, A. Figoli, Removal of dye from a leather tanning factory by flat-sheet blend ultrafiltration (UF) membrane, Membranes (Basel), 10 (2020) 47, doi: 10.3390/membranes10030047.

[71] R.J. Kadhim, F.H. Al-Ani, M. Al-Shaeli, Q.F. Alsalhy, A. Figoli, Removal of dyes using graphene oxide (GO) mixed matrix membranes, Membranes (Basel), 10 (2020) 366, doi: 10.3390/membranes10120366.

[72] D.D. Al-Araji, F.H. Al-Ani, Q.F. Alsalhy, Modification of polyethersulfone membranes by polyethyleneimine (PEI) grafted silica nanoparticles and their application for textile

wastewater treatment, Environ. Technol., (2022) 1–17, doi: 10.1080/09593330.2022.2049890.

[73] M. Abdul-Majeed, A.N. Ahmed, M. Al-Furaiji, I. Ghazi, Effect of adding arabic gum and zinc oxide nanoparticles to MBR membranes supported by carbon nanotubes for ultrafiltration process of dairy wastewater, Pollution, 8 (2022) 1233–1249.

[74] M.K. Paidi, V. Polisetti, K. Damarla, P.S. Singh, S.K. Mandal, P. Ray, 3D natural mesoporous biosilica-embedded polysulfone made ultrafiltration membranes for application in separation technology, Polymers (Basel), 14 (2022) 1750, doi: 10.3390/polym14091750.